Search for Lorentz invariance violation using gamma-rays from Markarian 421

Blažević, Luka

UNIVERSITY OF RIJEKA
FACULTY OF PHYSICS

Luka Blažević

Search for Lorentz invariance violation using gamma-rays from Markarian 421

Master thesis

Rijeka, 2023.

UNIVERSITY OF RIJEKA
FACULTY OF PHYSICS

Master's degree in physics

Astrophysics and physics of elementary particles

Luka Blažević

Search for Lorentz invariance violation using gamma-rays from Markarian 421

Master thesis

Mentor: izv. prof. dr. sc. Tomislav Terzić

Rijeka, 2023.

ABSTRACT

Measurements of quantum gravity could be made by looking at some of the proposed quantum gravity effects, such as fluctuations of space-time. The Lorentz invariance violation (LIV) effect appears as a consequence of the modified photon dispersion relation, used to model the effect of space-time fluctuations on gamma rays. Using the LIV time of flight analysis, we are able to look for quantum gravity effects using observations at energies much lower than the Planck scale. One of the most popular methods for the LIV time of flight analysis is the maximum likelihood method.

In this thesis, we focused on looking at how the choice of the function used to create the light curve template affects the maximum likelihood analysis. The functions used were: i) sum of Gaussian distributions, ii) sum of Cauchy distributions, iii) sum of skewed Gaussian distributions, iv) Fourier series, v) Kernel density estimation. This analysis was based on simulations of observations of Markarian 421 on the night of 24 to 25 of April 2014, preformed by Major Atmospheric Gamma Imaging Cherenkov (MAGIC) telescopes.

Fourier series and Kernel density estimation were not able to achieve a satisfying fit of the observed data, so their light curves were not used for the final maximum likelihood analysis. For the other functions, the fits managed to capture the structure of the light curve with more accuracy. Furthermore, their χ^2 tests were very similar, so they made good candidates for comparison.

The recreated light curves were then used in the `LIVelihood` software for LIV time of flight studies. Using simulations, LIV parameter λ was calculated along with the respective upper and lower limits to form a 95 % confidence interval. The light curve template created using the sum of skewed Gaussian distributions was not converging in enough simulations for the λ distribution to be calculated. For the light curve templates created using the sum of Gaussian distributions and the sum of Cauchy distributions λ was calculated to be $(-139.9 \pm 875)\,\mathrm{s/TeV}$ and $(-76.22 \pm 971)\,\mathrm{s/TeV}$, respectively. In addition, the lower limit on the energy at which the effects of quantum gravity become significant in the linear term were calculated from λ and amount to $E^{(G)}_{\mathrm{QG}_1} = 2.48557 \cdot 10^{17}\,\mathrm{GeV}$ and $E^{(C)}_{\mathrm{QG}_1} = 3.11314 \cdot 10^{17}\,\mathrm{GeV}$ for the sum of Gaussian distributions and the sum of Cauchy distributions light curve templates, respectively.

SAŽETAK

Kvantna gravitacija bi semogla mjeriti pomoću nekih od predloženih efekata kvantne gravitacije, kao na primjer fluktuacije prostor-vremena. Efekt narušenja Lorentzove simetrije (LIV) pojavljuje se kao posljedica modificirane disperzijske jednadžbe fotona, koja se koristi za modeliranje efekta fluktuacija prostor-vremena na gamma-zrake. Koristeći LIV analizu vremena leta, možemo promatrati efekte kvantne gravitacije koristeći opažanja na energijama puno nižim od Planckove skale. Jedna od najpopularnijih metoda za LIV analizu vremena leta je *maximum likelihood* metoda.

U ovom radu fokusiramo se na promatranje kako odabir funkcije kojim se kreira uzorak svjetlosne krivulje utječe na *maximum likelihood* analizu. Funkcije koje smo koristili su: i) suma Gaussovih raspodjela, ii) suma Cauchy raspodjela, iii) suma asimetričnih Gaussovih raspodjela, iv) Fourierov red, v) *Kernel density estimation* (KDE). Ova analiza je bila bazirana na simulacijama opažnja Markariana 421 u noći od 24. do 25. travnja 2014., s *Major Atmospheric Gamma Imaging Cherenkov* (MAGIC) teleskopima.

Prilagodbe podataka s Fourierovim redom i KDE-om nisu dale zadovoljavajuće rezultate te ih nismo koristili u konačnoj analizi. Ostale funkcije su puno bolje prikazale strukturu podataka. Također rezultati njihovih χ^2 testova su međusobno jako slični što znači da smo ih mogli pouzdano uspoređivati.

Svjetlosne krivulje dobivene iz prilagodbe smo zatim koristili u `LIVelihood` softveru za LIV analizu vremena leta. Koristeći simulacije izračunali smo LIV parametar λ skupa s njegovim gornjim i donjim granicama da bi dobili 95 % interval pouzdanosti. Distribucija parametra λ nije bila izračunata za svjetlosnu krivulju dobivenu iz sume asimetričnih Gaussovih raspodjela jer minimum nije konvergirao u dovoljno simulacija. Za svjetlosne krivulje dobivene iz sume Gaussovih raspodjela i Cauchyevih distribucija vrijednost parametra λ iznosi $8 - 139.9 \pm 875)\,\mathrm{s/TeV}$ i $(-76.22 \pm 971)\,\mathrm{s/TeV}$, respektivno. Za kraj pomoću parametra λ izračunate su donje granice vrijednosti energije na kojoj efekti kvantne gravitacije postaju signifikantni u linearnom članu i one iznose $E^{(G)}_{\mathrm{QG}_1} = 2.48557 \cdot 10^{17}\,\mathrm{GeV}$ za sumu Gaussovih raspodjela i $E^{(C)}_{\mathrm{QG}_1} = 3.11314 \cdot 10^{17}\,\mathrm{GeV}$ za sumu Cauchyevih distribucija.

Contents

1 INTRODUCTION

The need for a quantum formulation of the theory of gravity arises while looking at some of the extreme phenomena in the universe, such as the very beginning of the universe or some results of the general theory of relativity, such as the singularities of black holes. In these cases, the classical formulation of the theory of gravity based on the general theory of relativity breaks down, and a more fundamental theory is required to describe these phenomena. This new description comes in the form of theory of quantum gravity. While there have been many attempts to formulate a working theory of quantum gravity using different approaches (see, e.g. [1, 2, 3, 4, 5, 6]), a consistent theoretical formulation has not yet been proposed. One of the challenges in coming up with a robust theoretical foundation for quantum gravity is the lack of experimental result and measurements that would help guide the theoretical efforts. This is because the expected scale at which the quantum gravity could be measured is the Planck scale ($E_{Pl} \approx 1.22 \cdot 10^{19}$ GeV). Presently, we are not able to reach anywhere near those energies using terrestrial particle accelerators. That leaves us with using extraterrestrial accelerators such as active galactic nuclei (AGN), pulsars, gamma-ray bursts, etc. But even then the highest energy particles observed so far are cosmic rays at energies $\sim 3.2 \cdot 10^{11}$ GeV [7, 8], which is still several orders of magnitude too low. Other sources such as gamma rays have even lower energies at $\approx 1.4 \cdot 10^{6}$ GeV [9]). Despite these limitations, there could still be a way to measure the effects of quantum gravity.

One of the proposed quantum gravity effect would be fluctuations of space-time on the Planck scale. These fluctuations would affect photons with energies much lower than the Planck scale, which can then be used to measure the effects of quantum gravity. The effect of fluctuation on photons can be modelled with a modified photon dispersion relation. The modification of the photon dispersion relation leads to a change in the photon group velocity in vacuo. The new group velocity is energy dependent, which means that the photons of different energies travel at different velocities in vacuo. This now violates the Lorentz symmetry. However, these effects are suppressed by the order of energy they appear at. Being on the Planck scale severely limits the effects of this modification, but since the effect is cumulative it can still have significant consequence for great distances. Photon energy also plays a key role in the significance of the effect, with higher energy photons experiencing a bigger change in the group velocity.

In this thesis, we searched for the Lorentz invariance violation (LIV) by comparing the

arrival times of photons with their temporal distribution at the source. If the LIV effect is present, there should be a difference in the arrival time as a consequence of the change in their time of flight as a result of the modification in the dispersion photon relation. For the analysis, we used gamma rays emitted from Markarian 421, observed by Major Atmospheric Gamma Imaging Cherenkov (MAGIC) telescopes during a strong flare on the night of 24 to 25 of April 2014. The photon temporal distribution needed to be recreated. With the telescope, we are only able to detect the light curve as it looks like on Earth. Without LIV, that light curve would be the same at the source. However, the LIV effect is the result of the change in photon speed, meaning that the light curve would change over time as we move from the source to the detector. To recreate the light curve at the source, we created a light curve template by fitting observed low energy gamma rays with different functions. In the context of this thesis, we considered that the low energy gamma rays are the ones with energies in the range from 100 to 200 GeV. For fitting the light curve, we used several different functions: i) sum of Gaussian distributions, ii) sum of Cauchy distributions, iii) sum of skewed Gaussian distributions, iv) Fourier series v) Kernel density estimation. The resulting distribution were then used as inputs in `LIVelihood` software. `LIVelihood` was developed by Bolmont et al. [10] to allow LIV time of flight analysis from multiple sources and observatories.

The idea behind using different functions was to compare the results of the fit and see which method gave us a more optimised maximum likelihood analysis. For the fit, functions attempted to use functions that gave the similar fit as determined by χ^2 test. The first criteria was to determine whether the maximum likelihood would converge for a given function. Secondly, we compared the result to see which function managed to give us the narrowest confidence interval for the LIV parameter. Furthermore, we looked at which function would compute the maximum likelihood in the shortest time. Finally, we compared the complexity of the fit functions. If a function is too complex, it might be difficult to make a fit that converges.

2 LORENTZ INVARIANCE VIOLATION

As mentioned before, a proposed effect of quantum gravity is fluctuation of space-time on the Planck scale. To model the effect of these fluctuations, we can introduce a modified photon dispersion relation:

$$E^2 = p^2c^2 \times \left[1 + \sum_{n=1}^{\infty} \pm \left(\frac{E}{E_{\mathrm{QG},n}}\right)^n\right] \tag{1}$$

where E is the photon energy, p is the photon momentum, c is the standard speed of light, $E_{\mathrm{QG},n}$ is the energy at which the effects of quantum gravity become significant and n order in the expansion. So far, only the lower limits have been set on $E_{\mathrm{QG},n}$ and depending on the n used the limits are different. Limits vary based on the observed source and analysis methods, but for example, the limits from Markarian 501 observations are $E_{\mathrm{QG},1} = 2.1 \cdot 10^{17}\,\mathrm{GeV}$ and $E_{\mathrm{QG},2} = 2.6 \cdot 10^{10}\,\mathrm{GeV}$ [11]. For $n = 1$, we get the linear term, which is usually considered first. In the event that the contribution of the linear term is negligible, meaning $E_{\mathrm{QG},1} \to \infty$, the quadratic term ($n = 2$) is considered. Since the energy $E_{\mathrm{QG},n}$ is around the order of Planck scale, going beyond the quadratic term would require very high photon energies E for the term to be significant. Because of this, experiments usually focus on the linear and quadratic term.

The modification of the photon relation then results in the change of the photon group velocity in vacuo:

$$v_g = \frac{\partial E}{\partial p} \cong c\left[1 + \sum_{n=1}^{\infty} \pm \frac{n+1}{2}\left(\frac{E}{E_{\mathrm{QG}}}\right)^n\right] \tag{2}$$

The $+$ and $-$ cases correspond to speeds greater than c (superluminal) and smaller than c (subluminal), respectively.

Lorentz symmetry is the invariance on Lorentz transformations. That invariance guaranties that all photons have the same velocity in vacuo regardless of direction of emission or the mutual speed of the source and the observer. The modification of the photon dispersion relation (1) and the consequent energy dependence in the photon group velocity in vacuo (2) leads to a violation of the Lorenz invariance, meaning photons of different energies travel at different speeds in vacuo. For two photons with energies $E_h > E_l$ emitted at the same time, the difference in arrival time can be expressed as:

where Δt_d is the detection interval and Δt_{LIV} difference in time of flight given by:

$$\Delta t_n = \pm \frac{n+1}{2} \frac{E_h^n - E_l^n}{H_0 E_{\mathrm{QG}}^n} \int_0^z \frac{(1+z')^n}{\sqrt{\Omega_\Lambda + \Omega_m (1+z')^3}} dz' \tag{3}$$

where $H_0 = (67.4 \pm 0.5)\mathrm{kms}^{-1}\mathrm{Mpc}$ the Hubble constant, $\Omega_\Lambda = 0.685 \pm 0.007$ the dark-energy density parameter and $\Omega_m = 0.315 \pm 0.007$ the matter density parameter are cosmological parameters of the ΛCDM model [12] and z source redshift [13]. This effect can be positive or negative depending on the sign used in the photon group velocity, resulting in propagation in vacuo faster or slower than the standard speed of light. This effect is cumulative, which means that the photons emitted by sources that are further away from us would exhibit a stronger change in their time of flight. The effect is also energy dependant, meaning that higher energy photons display a greater time of flight change.

For later use in analysis, from equation (3), we can define another parameter λ_n as:

$$\lambda_n = \frac{\Delta t_n}{(E_h^n - E_l^n) \int_0^z \frac{(1+z')^n}{\sqrt{\Omega_\Lambda + \Omega_m (1+z')^3}} dz'} = \pm \frac{n+1}{2 H_0 E_{\mathrm{QG}}^n} \tag{4}$$

Parameter λ_n is independent of the source distance and represents the time delay in s/TeV. As seen from equation (3), the LIV effect leads to a change in the temporal distribution of the photons at the detector compared to the temporal distribution at the source. The existence of the LIV effect can therefore be verified by checking if the detected photons match their distribution at the source.

3 ANALYSIS METHOD

Presently, one of the most popular methods for LIV time of flight analysis is the maximum likelihood method, see e.g. [14].

3.1 Light curve template

In general, we are not able to know the exact time of emission for an individual gamma ray, we can only put constraints on the emission times based on the variability in the flux. For periods where flux is increased, there is a greater chance of a photon emission during that time. This means that if we have a flux that is highly variable, we can have a more strongly constrained temporal distribution of emitted photons. In addition, we are not able to obtain a light curve directly at the observed source. We are limited in observations to the light curve obtained directly at the detector. This poses a problem because to test for the existence of the LIV effect we need to know the temporal distributions of the photons at the source of the emission. To overcome this problem, we needed to recreate the photon temporal distribution at the source using the observed light curve. We achieved this by creating a light curve template. The light curve template is a probability distribution function of gamma ray emission times. To create the light curve template, we fit the observed light curve with a function of our choice. However, we only fit the photons for which the LIV effect is negligible. For those photons, the distribution did not change while they were travelling from the source to the detector. Then we assume that all the photons at the source were distributed in this way, which then gives us the temporal distribution of the photons at the source before any possible LIV effects.

Since we need a highly variable flux, the structure of the resulting light curve is complex. This makes creating the light curve template difficult. Firstly, we need enough data to make sure the light curve is properly fitted. If we use too little data, the resulting light curve template might not be an accurate representation of the source light curve. Secondly, the choice of the function used for the fit is important. Some functions might create a more accurate light curve template, but once used as the input for maximum likelihood estimation fail to converge, or might take a long time to process. Because of this, we are using 5 different functions for the fit. We can then compare how each function preforms by looking at which functions give the narrowest confidence interval for the LIV parameter, has

a faster computing time, and if some do not converge at all.

3.2 Extracting the signal

Gamma-ray observations with terrestrial telescopes are made by detecting the Cherenkov radiation resulting from the extensive air showers induced by their interaction with the Earth's atmosphere. When a gamma ray or a cosmic ray hits the atmosphere, it splits into an electron positron pair. These electrons and positrons create more gamma rays, which produce more electron positron pairs and so on. If the electrons or positrons are travelling faster than the speed of light in the air, they emit Cherenkov radiation. This radiation is then detected by the telescopes. The resulting observations are then used to recreate the energy and origin of the initial gamma ray or cosmic ray that interacted with the atmosphere. This makes it difficult to know for sure if the detected event is a gamma ray or a cosmic ray. In addition, not all detected gamma rays are emitted from the observed source. Some come from other sources and make up the background noise.

To make the analysis more accurate, we need to subtract the background from the source signal. The first step in doing so if defining the ON and OFF regions in the field of view. The ON region is a circular area in the camera around the source position in the camera. It contains events from the observed source as well as the background noise. The OFF region is a circular area in the camera adjacent to ON region. It contains just the background. The number of events in the ON region is labelled by N_{ON}, while the number of events in the OFF region is labelled by N_{OFF}. By subtracting the number of ON and OFF events, we are left with the number of excess events, i.e. N_{EX}. This is an approximate number of events emitted by the source. We are not able to know the exact number of signal events without the background because we are not able to differentiate between the signal and background events in the ON region.

3.3 Maximum likelihood

Maximum likelihood estimation is a statistical method of estimating the value of a parameter λ, which follows an assumed probability distribution, so that the estimated value $\hat{\lambda}$ maximises the likelihood function $\mathcal{L}(\mathbf{X}|\theta)$ for a particular observation $\mathbf{X}$. The likelihood function of a

set of N independent observations $\mathbf{X} = X_1, X_2, ..., X_N$ is given by:

$$\mathcal{L}(\mathbf{X}|\lambda) = \prod_{i=1}^{N} f(X_i, \lambda) \tag{5}$$

where $f(X_i, \lambda)$ is a probability distribution function of any observation X_i [15].

3.3.1 Maximum likelihood in LIV analysis

For the use in LIV time of flight analysis, the likelihood function $\mathcal{L}$, for N_{ON} observed events from the ON region, is given by:

$$\mathcal{L}(\lambda_n) = \prod_{i=1}^{N_{\mathrm{ON}}} \left(p_i^{(s)} \frac{f^{(s)}(E_i, t_i)}{\int_{E_{min}}^{E_{max}} \int_{t_{min}}^{t_{max}} f^{(s)}(E,t)\, dtdE} + p_i^{(b)} \frac{f^{(b)}(E_i, t_i)}{\int_{E_{min}}^{E_{max}} \int_{t_{min}}^{t_{max}} f^{(b)}(E,t)\, dtdE} \right) \tag{6}$$

where $p_i^{(s)}$ and $p_i^{(b)}$ are the probabilities for the event i to be either the signal or the background, respectively, since the ON region contains gamma rays from the source and the background. The energies E_i are in the ranger of the minimum and maximum energy observed, and the times t_i are in the range from the start to the end of the observation. Maximum and minimum energy and times are used for normalisation of the signal and background parts of the likelihood function. $f^{(s)}(E,t)$ is the probability distribution function for detecting a gamma ray with energy E at the time t and $f^{(b)}(E,t)$ is the probability distribution function for detecting a background event with energy E at the time t. The probability distribution function for detecting a gamma ray with energy E at the time t can be calculated with:

$$f^{(s)}(E,t) = \int_0^{\infty} F(t)\Phi_{obs}(E)G(E, E_{true})A_{eff}(E_{true}, t)dE_{true} \tag{7}$$

where $F(t)$ is the light curve template, $\Phi_{obs}(E)$ is the observed spectral distribution of gamma-rays, $G(E, E_{true})$ term represents the energy resolution and the instrument bias. E_{true} is the true energy of a particular event, while $G(E, E_{true})$ is the probability distribution function of E_{true} being measured as E. Lastly, $A_{eff}(E_{true}, t)$ is the collection area of the instrument in true energy. The collection is also a probability distribution function and represents a probability that we detect an event of that energy. It can be time dependant if the observation conditions are variable. The same expression (equation (7)) is used for the background events probability distribution function but with slightly different considerations. Since, in general, we are not able to determine the origin of the background events their energy and time distribution are taken to be the same as observed on Earth, unlike gamma

rays where we take the distribution at the source. Probabilities for the event to be part of the background or the signal can be calculated with:

$$p_i^{(s)} = n\frac{N_{\mathrm{ON}} - \alpha N_{\mathrm{OFF}}}{N_{\mathrm{ON}}} \quad , \quad p_i^{(p)} = \frac{\alpha N_{\mathrm{OFF}}}{N_{\mathrm{ON}}} \tag{8}$$

α is the ratio of effective exposure time in the ON and OFF regions ($\alpha = t_{\mathrm{ON}}/t_{\mathrm{OFF}}$).

3.4 LIVelihood

`LIVelihood` software is used to calculate the maximum likelihood of the LIV parameter λ_n and reconstruct the lag of the photons. The calculation is done by preforming simulations of the source based on the provided light curve template and parameters which characterise the source. Parameters needed for the simulations are: i) time range of the observation, ii) energy range of the observed photons, iii) light curve template, iv) photon energy distribution, v) proportion of the background signal, vi) redshift of the source.

For provided parameters, `LIVelihood` constructs N simulations of the source. For each simulation, the log-likelihood is calculated using the logarithm of the equation (6). The minimum of the log-likelihood function gives us the value of the parameter λ_n which maximises the likelihood function. The upper and lower 95 % confidence interval limits are taken as the point where:

$$-2\ln\mathcal{L}(\lambda_n) = 3.84 \tag{9}$$

The final value of the LIV parameter, with the respective upper and lover limits, is calculated as the mean of the N simulations. The lag is also reconstructed by fitting an asymmetrical Gaussian distribution over the LIV parameters given from each simulation.

4 DATA SAMPLE

There are several types of gamma-ray sources that could be used for LIV tests. Pulsars have a regular pulsation, which would allow using signals from different periods, providing us with large data samples. The downside is their relative proximity to Earth, which greatly reduces the possible LIV effect, making it hard to detect. Gamma-ray bursts have a short variability timescale which is useful in LIV testing, but are very unpredictable and because of their great distance from the Earth a lot of very high energy gamma rays end up being absorbed on the way. Lastly, AGN-s can have strong flares with high variability and flux, which in addition to being relatively easy to detect makes them great candidates for LIV time of flight analysis.

For this analysis, we used gamma rays from an AGN Markarian 421 observed by the MAGIC telescopes on the night from 24 to 25 of April 2014. Data came in the form of DL3 files, from which we extracted the events. DL3 is a standardised format for storing high-level astronomical gamma-ray data. They contain an event list consisting of gamma-like events and the instrument response function (IRF). The event list is made after the analysis cuts. The analysis cut is made to keep only gamma-ray like events and discard those that can safely be considered as part of the background noise. The IRF contains the effective area, energy dispersion and the point spread function of the instrument.

4.1 Markarian 421

Markarian 421 an AGN (BL Lac) located in the Ursa Major constellation at the redshift $z = 0.0308$. It is one of the brightest blazars, making it also one of the most observed objects in the very high energy range. Observations of Markarian 421 have been made in the whole electromagnetic spectrum from various different telescopes. Along with having a very high flux, it also shows rapid flux variability [16].

As stated before, sources with a high flux variability are very important in LIV time of flight analysis. The strength of the flux also plays a significant role in the analysis. Stronger flux provide richer sample statistics, especially on the higher energies where the LIV effect is more pronounced.

Because of this, we selected Markarian 421 as the observed source. Specifically, MAGIC observations on the night from 24 to 25 of April 2014 when it experienced a strong flare.

The observation was scheduled to last from 22h25 to 22h55. When the flare started, the observation was extended, so the flare could be observed in its entirety. In the end, the whole observation lasted for about three and a half hours. Maximum intensity of the flux was 7 CU, after which it decreased to 2 CU for the rest of the observation. CU is the intensity of the flux in the units of Crab Nebula flux. The observation was done in wobble mode. When the wobble mode is used [17], the telescope does not point directly at the source but slightly next to it. This is done to allow for a simultaneous observation of the background and the source. Using this observation mode, the amount of time needed to make background estimation is greatly reduced, since we no longer need to make a separate observation to get data from the background. To account for the asymmetries in the camera and the observed background after the first run, the pointing position of the telescope is shifted to the position opposite to the initial one with respect to the source. For this particular observation, 13 runs were made, each lasting approximately 15 minutes. For the observation, the zenith angle ranged from 10° to 50°. Weather conditions for the duration of the flare were good, and no cloud cover was reported [18].

4.2 Data selection and analysis

Each event from the observations has a time of detection, reconstructed energy of the gamma ray and reconstructed coordinates of the origin of the gamma-ray. This information was used to determine which events we were going to use to create the light curve template. The first step in preparing the data was extracting events with energies between 100 and 200 GeV. The lower limit partially stems from the need to have a stable collection area of the detector. For energies lower than 100 GeV, the collection area changes significantly depending on the energy of the gamma ray, making the reconstructed gamma-ray energy unreliable. For similar reasons, we decided to limit our data to only the first 9 runs of the observation. This is because during the observation the zenith angle was increasing and with it the analysis energy threshold. With a higher zenith angle, the observed Cherenkov radiation emitted by the gamma rays has to travel through more of the atmosphere. While travelling through the atmosphere, the radiation can be scattered or absorbed. Cherenkov radiation caused by lower energy gamma rays has a higher chance of being scattered or absorbed. Meaning that making observations at a higher zenith angle raises the minimum energy of the gamma ray that can be observed, and in turn raises the minimum energy at which the collection

area is stable. To keep the energy range consistent for the whole observation, we focused only on the first 9 wobbles where the zenith angle was up to 35°. The 200 GeV upper limit was set as a compromise between the number of events used for the light curve template and the energy at which the LIV effect is no longer negligible. If the upper limit was too low, we would not have enough data to make an accurate light curve template and, on the other hand, if we set the upper limit too high we would no longer be able to ignore the LIV effect for those events. The energy limits are not strictly defined, and while we could have set them differently, we decided to use the 200 GeV limit since it is roughly the median of energy in the data.

The next step was defining the size of ON and OFF regions in the observations. For calculating the ON region, we used a `gammapy` function `CircleSkyRegion`, which uses the pointing coordinates of the telescope, source coordinates and angle from the "RAD MAX" table in the FITS files to calculate the size and location of the region for each energy range in the "RAD MAX" table. The OFF region is made by mirroring the ON region using the `gammapy` function `ReflectedRegionsFinder` for the same pair of energy ranges. Each event was then sorted into one of the two regions based on their origin coordinates. If an event was not inside one of the two regions, it was discarded from the analysis.

Now that we had extracted the events based on their energies and separated them in the ON and OFF regions, the final step of data selection was subtracting the background from the source events leaving us with an approximate number of events from the source. To do this, we binned the ON events in a way that each bin contained the same number of events, which makes all the bins have different widths ($w_i; i = 1, ..., N$ where N is the number of bins). The OFF events were then sorted into bins of the same widths w_i, but unlike the ON events, they have a variable number of events in each bin. By subtracting each ON and OFF bin, we were left with a number of events in each bin N_{EX}. The number of excess events N_{EX} is an approximate number of the events that make up the signal. We are not able to exactly know which event belongs to the signal and which is a part of the background, so by using the ON and OFF regions we get an estimation of the signal. To make the light curve from these binned excess events, each bin centre was used as an x-axis value and the height of the bin, i.e. number of events in the bin, was used as the y-axis value. The points obtained were then normalised and their uncertainties were calculated as:

$$\sigma_i = \frac{\sqrt{N_{\mathrm{ON}i} + N_{\mathrm{OFF}i}}}{w_i} \tag{10}$$

where $N_{\mathrm{ON}i}$ is the number of ON events for that bin, $N_{\mathrm{OFF}i}$ number of OFF events, w_i is the width of the bin and $i = 1, ..., N$ is the bin index. The resulting plot is shown on Figure 1.

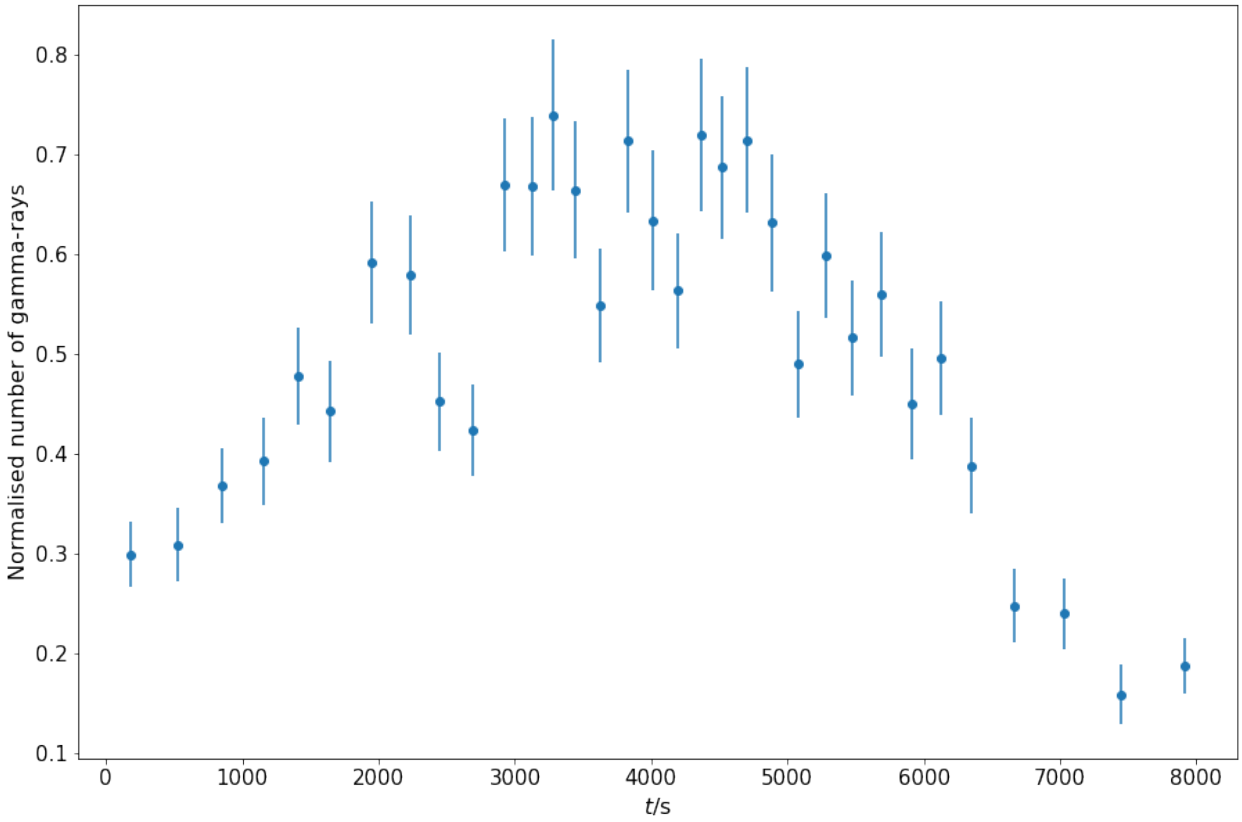

Figure 1: Light curve with bin centres used for x-axis, normalised number of events in the bin for the y-axis and uncertainties calculated using equation (10).

4.3 Light curve template

To create a light curve template that we would later on use in `LIVelihood` we fitted the light curve on Figure 1 with several functions. The functions used for fitting were:

- sum of Gaussian distributions

$$\Phi(t) = \sum_{i=1}^{N} \frac{A_i}{\sigma_i} \exp\left(-\frac{(t-\mu_i)^2}{2\sigma_i^2}\right) \tag{11}$$

- sum of Cauchy distributions

$$\Phi(t) = \sum_{i=1}^{N} \frac{A_i}{\pi \left(1 + \frac{(t-\mu_i)^2}{\sigma_i^2}\right)} \tag{12}$$

- sum of skewed Gaussian distributions

$$\Phi(t) = \sum_{i=1}^{N} \frac{A_i}{e^{\frac{\mu_i - t}{T_{ri}}} + e^{\frac{t-\mu_i}{T_{di}}}} \tag{13}$$

- Fourier series

$$\Phi_T(t) = \sum_{i=1}^{N} A_i \cos\left(i\frac{\pi}{T}t\right) \tag{14}$$

- Kernel density estimation (KDE)

$$\Phi_h(t) = \frac{1}{nh} \sum_{i=1}^{n} K\left(\frac{t - t_i}{h}\right) \tag{15}$$

Note that N is the number of functions used for fitting and n is the number of bins. All fits except the KDE were made using the `curve_fit` function from `SciPy` For KDE we used `KernelDensity` function from `sklearn.neighbors` in `python`.

We used several different functions for the fit so we could compare the results and see which function gives us the best fit while also keeping the number of parameter to a minimum. For the functions used in the final analysis, the number of parameters was 12 for all the functions, so that we could compare them to each other.

4.3.1 Kernel density estimation

Kernel density estimation uses kernel smoothing, i.e. estimates a real valued function as the weighted average of neighbouring data, in order to estimate the probability density function of a random variable using kernels (window functions) as weights. For the analysis we used `KernelDensity` function from `sklearn.neighbors` in `python`. This function gives a density estimate at a point y within a group of points $x_i; i = 1, ..., N$ as:

$$\Phi_K(y) = \sum_{i=1}^{N} K(y - x_i; h) \tag{16}$$

where $K(x; h)$ is a positive function (kernel) and is controlled by the bandwidth parameter h. For the fit, we used the Gaussian distribution kernel. Bandwidth parameter has a big influence on the result by changing the bias and variance of the estimate. High bandwidth

leads to smooth density distribution (high-bias) which hides the underlying structure of the data, making it difficult to draw any conclusions from the results. Small bandwidth leads to unsmooth density distribution (high-variance) which falsely shows more variation than is present in the data, which could lead to false conclusions. Since we were not able to justify the selection of the bandwidth parameter h, KDE method was not used in further analysis.

4.3.2 Fourier series

For the fit with Fourier series, we used function (14) with $N = 8$ and parameter T being the same for all terms of the sum ($T = 16800 \pm 70$). The `curve_fit` function did not converge if the uncertainties of the points were used in the fit, so to calculate the fit parameters and their standard derivations we ran the fit 500 times and each time fluctuated the y value of each point. By doing so, we simulated the uncertainties on each point. The fluctuation was done by taking the random value from the normal distribution centred on the original value of the point, with the standard deviation of the distribution given by the error of the point. Parameters were then taken as the average of the 500 runs and standard derivation calculated using the `std` function from `NumPy`.

To help visualise deviation of the fit to the data, three additional plots are made (Figure 2). The first one shows the distance of the fit function from the points with the original uncertainties on the points. Second shows the distance of the fit function from the points, divided by the uncertainties. Third shows the relative distance of the fit function from the points with the original uncertainties on the points, i.e. distance divided by the value of the points.

The resulting fit ended up being too smooth, meaning it did not manage to recreate the structure of the light curve with enough accuracy. This inaccuracy in the structure would make it difficult to draw any conclusion on the existence of the LIV effect. Additionally, as seen on the plots 2, 3 and 4 (Figure 2) deviation on some points is quite large. Because of this, the fit with Fourier series was not used in further analysis.

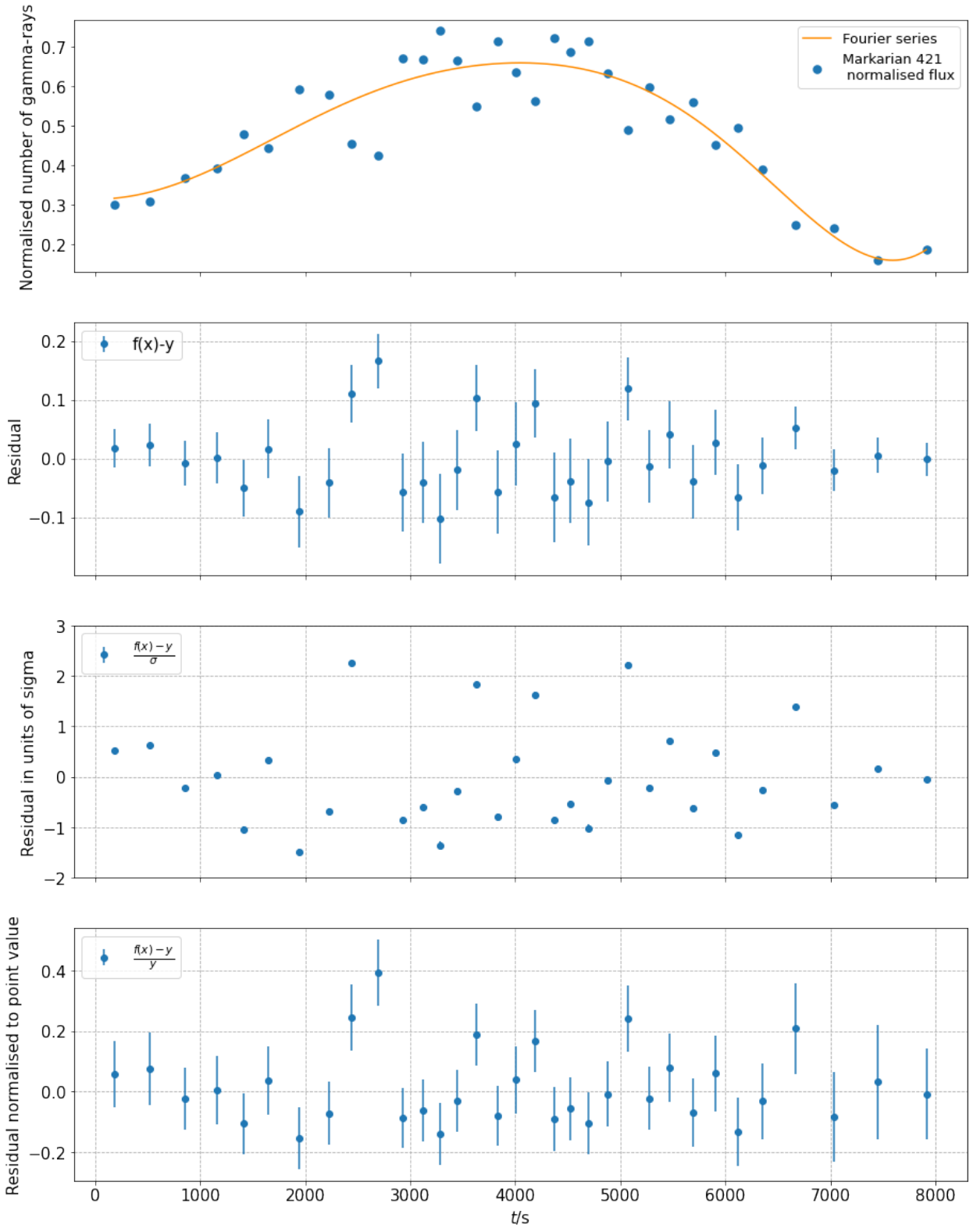

Figure 2: Light curve fitted with Fourier series and different residual representations. From top to bottom the pads show: i) Resulting fit with Fourier series (equation 14). ii) Residual with the uncertainties calculated from 500 fits with fluctuated y values of the points. iii) Residual in the units of σ with the same uncertainties used in second pad. iv) Residual normalised by points with normalised uncertainties from the second pad.

4.3.3 Sum of Gaussian distributions

The fitting was done using function (11) with $N = 4$. The fit results are shown in the table 1. Figure 3 shows the resulting fit, with individual Gaussian distributions that make up function (11) and the residuals, which are calculated in the same way as the Fourier series plot before. Since we are comparing different fit function to make sure they are similarly fitted, χ^2 was calculated and the results are shown in table 4.

For most of the points the residuals are within one sigma while none are exceeding two sigma. In contrast to the Fourier series plot, this plot recreated the light curve structure with more accuracy. Because of this the fit was later used as the light curve template for `LIVelihood` simulations.

Table 1: Fit parameters for the sum of Gaussian distributions, equation (11).

Parameter	Gauss 1 (red)	Gauss 2 (purple)	Gauss 3 (green)	Gauss 4 (pink)
A	63 ± 2024	353 ± 10505	132 ± 13729	330 ± 32549
μ	3198 ± 5894	1971 ± 87540	5917 ± 95444	4439 ± 36821
σ	227 ± 9709	1198 ± 79675	496 ± 37773	713 ± 133535

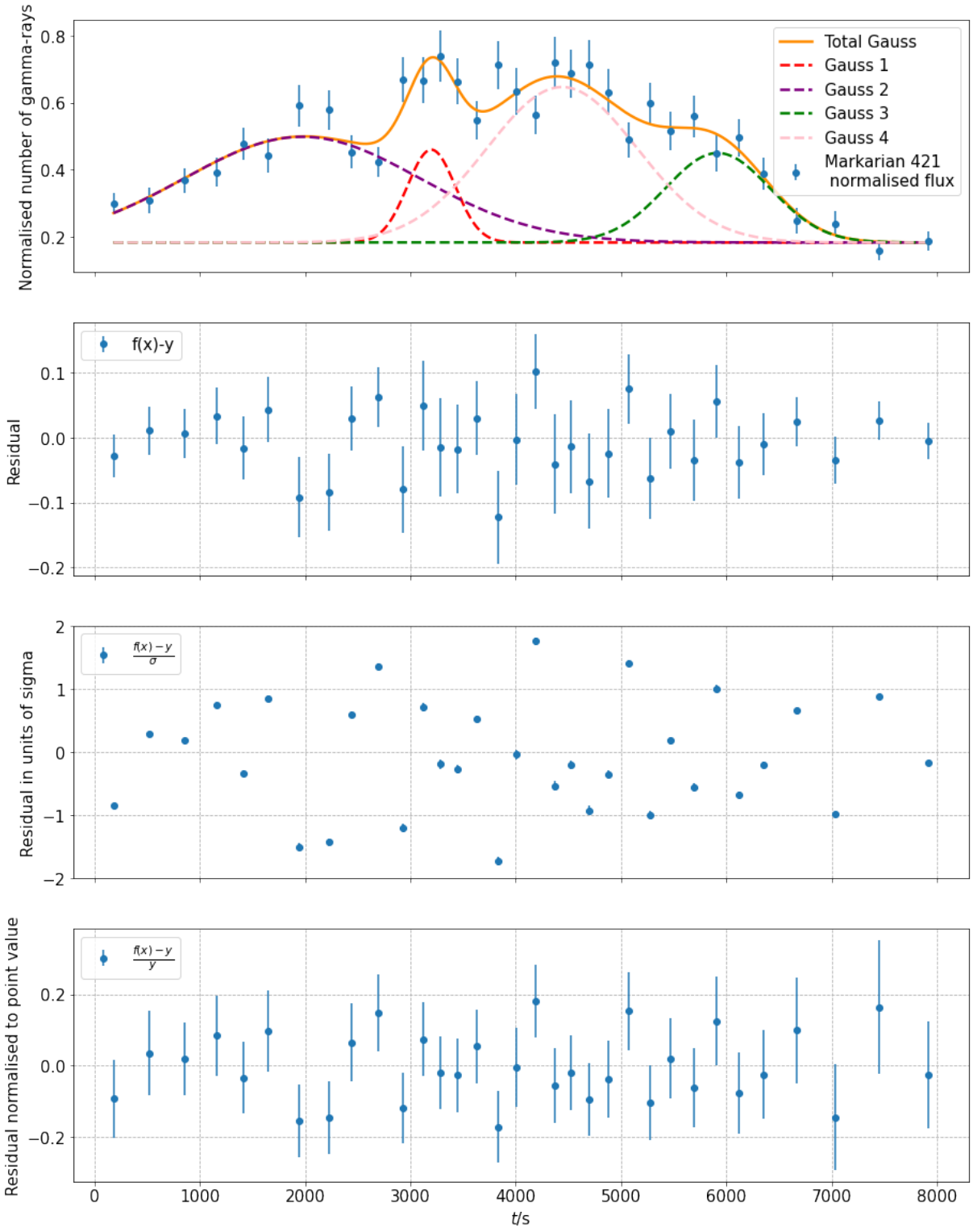

Figure 3: Light curve fitted with a sum of Gaussian distributions and different residual representations. From top to bottom the pads show: i) Resulting fit with individual Gaussian distributions that make up the sum (equation 11) and uncertainties on points calculated with equation (10). ii) Residual the same uncertainties as in the first pad. iii) Residual in the units of σ the same uncertainties as in the first pad. iv) Residual normalised by points with normalised uncertainties from the first pad.

4.3.4 Sum of skewed Gaussian distributions

The fitting was done using function (13) with $N = 3$. The fit results are shown in the table 2. Figure 4 shows the resulting fit, with individual skewed Gaussian distributions that make up function (13) and the residuals, which are calculated in the same way as the Fourier series plot before.

Similarly, as the Gaussian distribution fit, the residual for the most points is within one sigma with only one point exceeding two sigma. While one fewer term was used in comparison to the Gaussian distribution fit, the resulting χ^2 was similar, as shown in table 4. Since the resulting fit captured different aspects of the light curve structure compared to the Gaussian distribution fit, it made for a good comparison in the maximum likelihood results.

Table 2: Fit parameters for the sum of Gaussian distributions, equation (13).

Parameter	Skew Gauss 1 (red)	Skew Gauss 2 (purple)	Skew Gauss 3 (green)
A	0.5 ± 0.3	0.7 ± 0.6	1.2 ± 0.3
μ	2425 ± 10457	2890 ± 181757	4333 ± 249935
T_r	3544 ± 12608159	170 ± 22336	990 ± 1973093
T_d	93 ± 7088	524 ± 1403490	1726 ± 258025

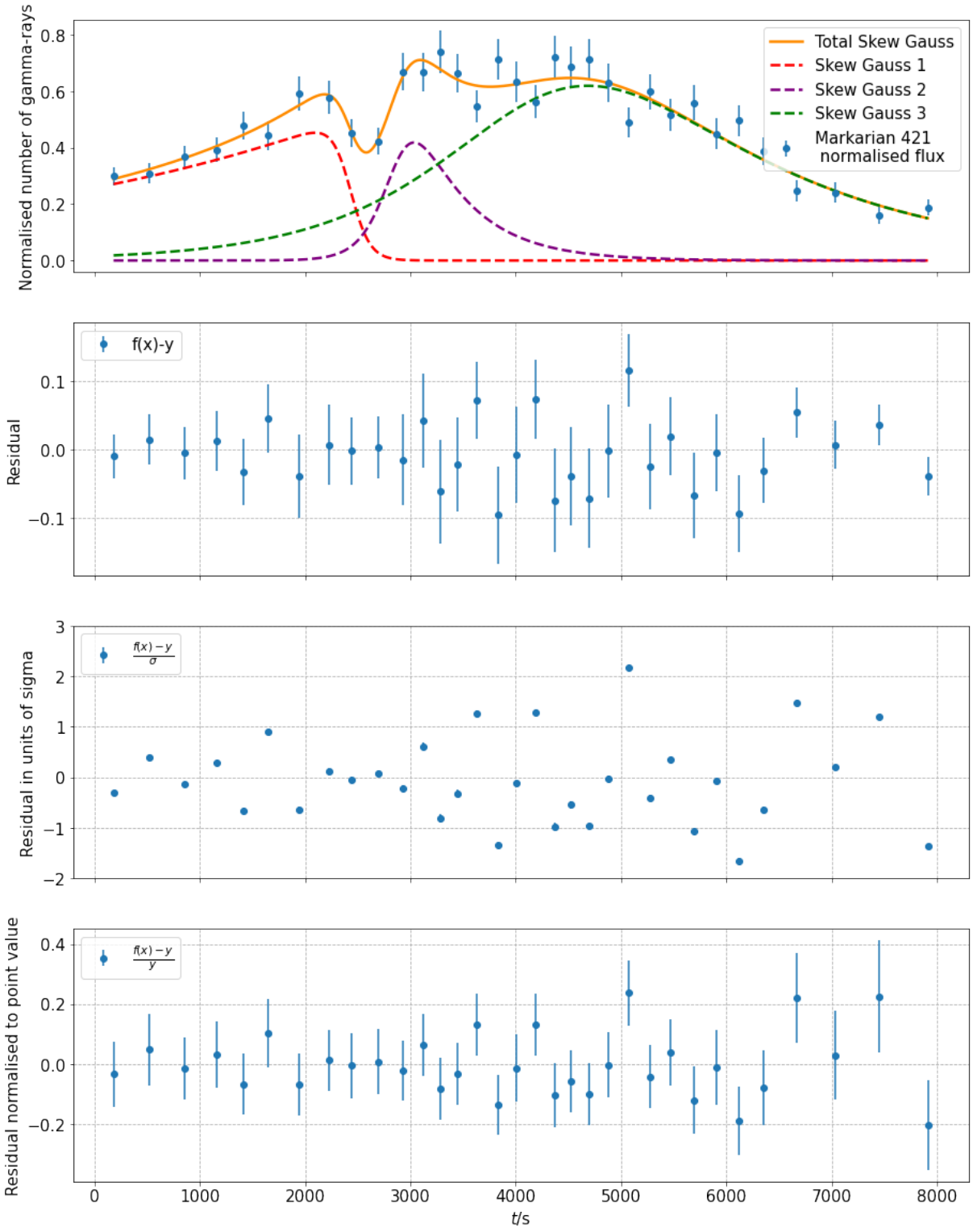

Figure 4: Light curve fitted with a sum of skewed Gaussian distributions and different residual representations. From top to bottom the pads show: i) Resulting fit with individual skewed Gaussian distributions that make up the sum (equation 13) and uncertainties on points calculated with equation (10). ii) Residual the same uncertainties as in the first pad. iii) Residual in the units of σ the same uncertainties as in the first pad. iv) Residual normalised by points with normalised uncertainties from the first pad.

4.3.5 Sum of Cauchy distributions

The fitting was done using function (12) with $N = 4$. The fit results are shown in the table 3. Figure 5 shows the resulting fit, with individual Cauchy distributions that make up function (12) and the residuals, which are calculated in the same way as the Fourier series plot before.

As well as the previous two fits, the residuals are mostly within one sigma, while none are above two sigma. Comparing the χ^2 results from the table 4 the Cauchy distribution had the worst results, but it was still very similar to the other fits. The resulting fit look similar to the Gaussian distibution fit, but since the functions used for fitting are very different, it still made for a good comparison in the maximum likelihood results.

Table 3: Fit parameters for the sum of Cauchy distributions, equation (12).

Parameter	Cauchy 1 (red)	Cauchy 2 (purple)	Cauchy 3 (green)	Cauchy 4 (pink)
A	1436 ± 287239	301 ± 54416	466 ± 164112	1205 ± 485140
μ	1774 ± 53155	3242 ± 6119	5856 ± 34077	4485 ± 19431
σ	1368 ± 177002	299 ± 34231	590 ± 117605	840 ± 171874

Table 4: χ^2 results for the fits.

	Gaussian distribution	Skewed Gaussian distribution	Cauchy distribution
χ^2	25.41	25.22	27
Reduced χ^2	1.27	1.20	1.37
p-value	0.19	0.24	0.12
Degrees of freedom	20	21	20

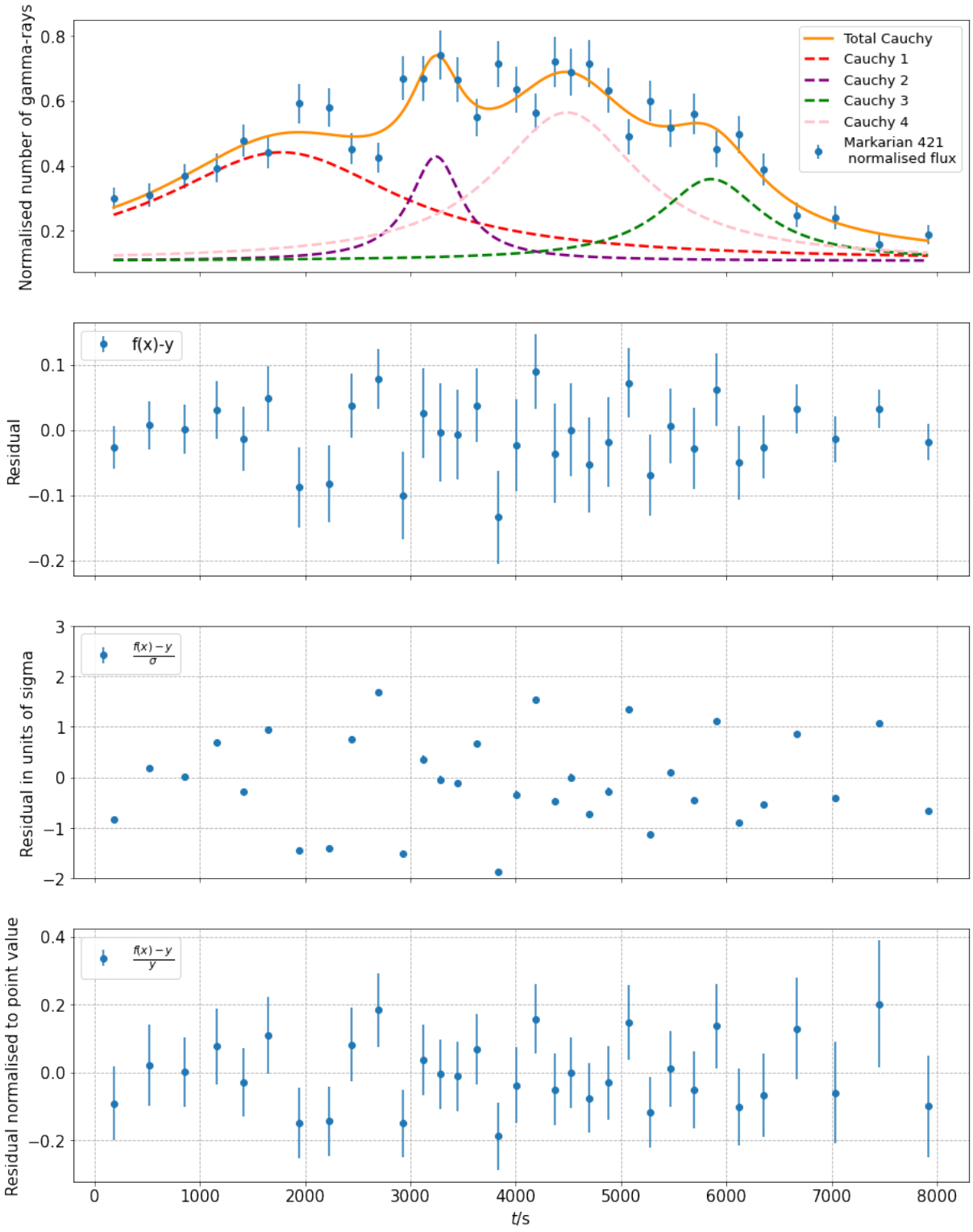

Figure 5: Light curve fitted with a sum of Cauchy distributions and different residual representations. From top to bottom the pads show: i) Resulting fit with individual Cauchy distributions that make up the sum (equation 12) and uncertainties on points calculated with equation (10). ii) Residual the same uncertainties as in the first pad. iii) Residual in the units of σ the same uncertainties as in the first pad. iv) Residual normalised by points with normalised uncertainties from the first pad.

5 RESULTS

For the maximum likelihood analysis, we assumed perfect resolution from the detector. This means there was no energy bias, i.e. in equation (7) the energy resolution and instrument bias term G is an identity matrix. Additionally, the collection area of the instrument is homogenous and constant in time and across the energy range. This was done because in this thesis we focused on comparing the likelihood results from different functions that were used to generate the light curve template. For that analysis, the detector systematics are not relevant and making the resolution perfect makes the analysis easier.

5.1 Example analysis

Before working on the data from Markarian 421 we preformed an example analysis using the data from the `LIVelihood` tutorial [19]. In the tutorial, the High Energy Stereoscopic System (HESS) observations of AGN PKS 2155-304 were used. The observation chosen was from the night of 29 to 30 of July 2006.

The data was fitted with a single Gaussian distribution:

$$\Phi(t) = A \exp\left(-\frac{(t-\mu)^2}{2\sigma^2}\right) + C \tag{17}$$

The resulting fit is shown on Figure 6. The fit was then used as the light curve template input for `LIVelihood` to preform simulations of the source. The first result of the simulation is the plot showing the likelihood value with respect to the time shift (Figure 7). From this plot we can take the upper and lover values of the time shift so that they make the 95 % confidence interval. The simulation was made 100 times and the resulting time shifts plotted as a histogram along with their upper and lover limits on Figure 8. On each plot there are additional information about the time shift: i) number of simulations, ii) mean and standard deviation of the 100 simulation results, iv) underflow and overflow, i.e. the number of results exceeding the boundaries of the plot, v) χ^2 and the number of degrees of freedom, vi) p-value, vii) parameters of the asymmetrical Gaussian distribution fit.

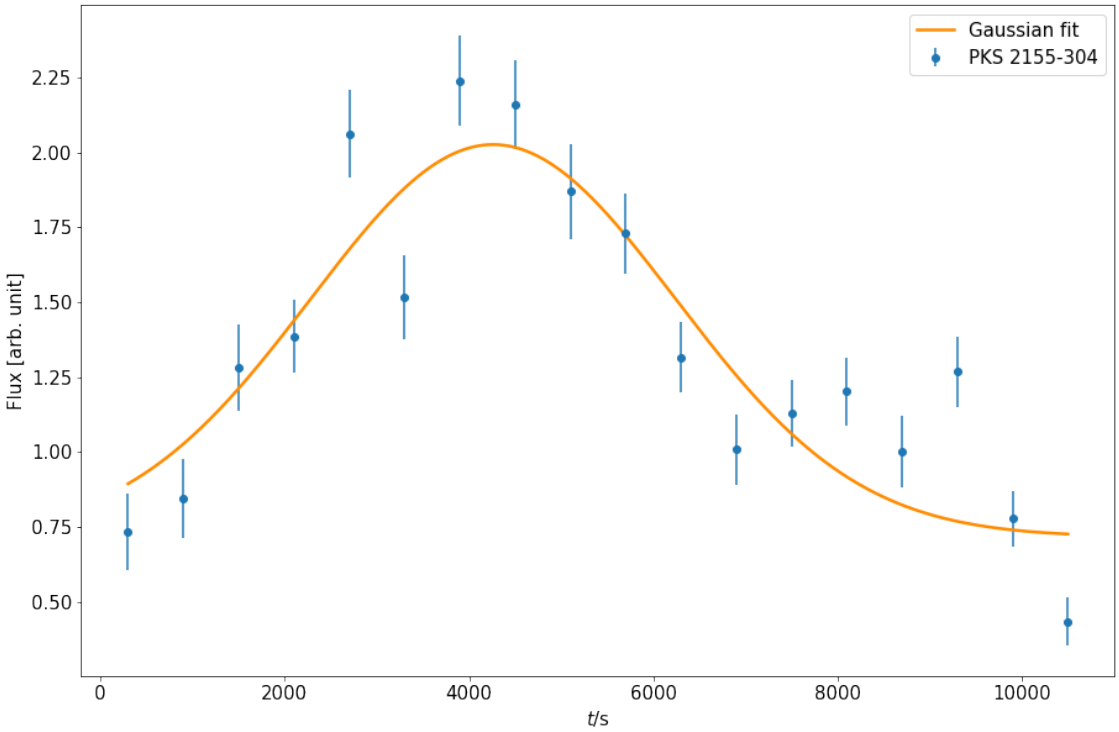

Figure 6: PKS 2155-304 light curve with a fitted Gaussian distribution, equation (17).

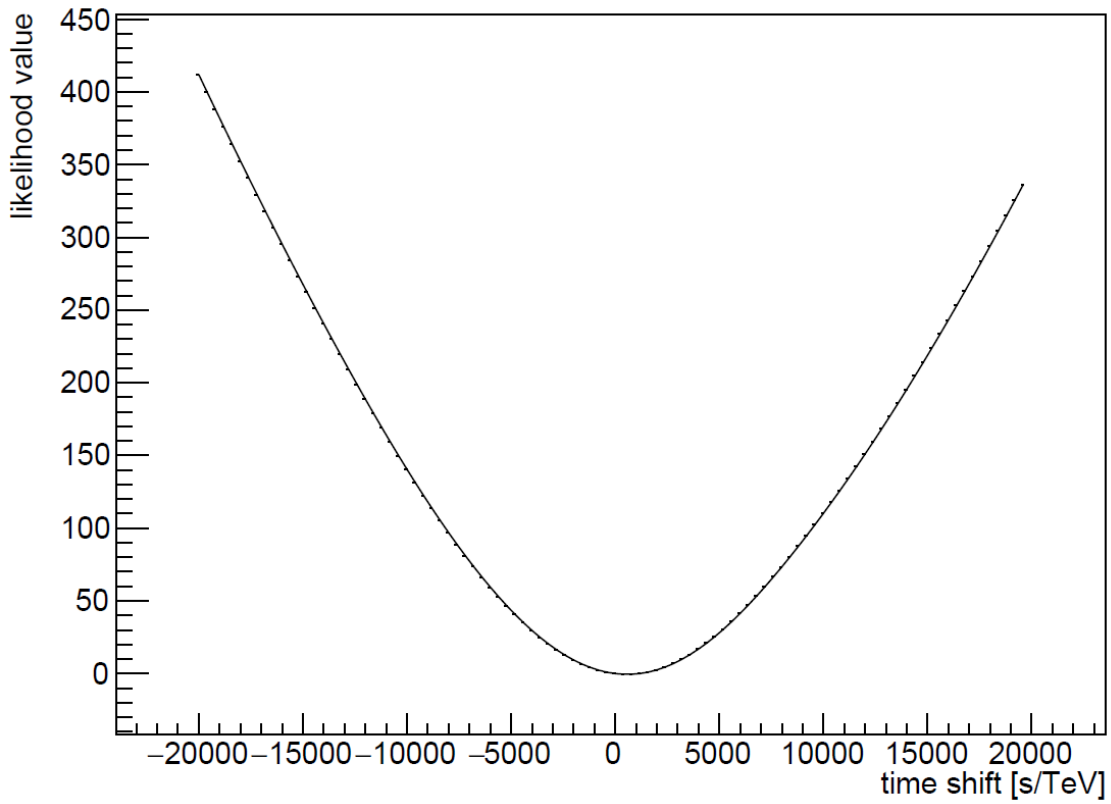

Figure 7: Likelihood value with respect to the timeshift for the example `LIVelihood simulation` of PKS 2155-304 data.

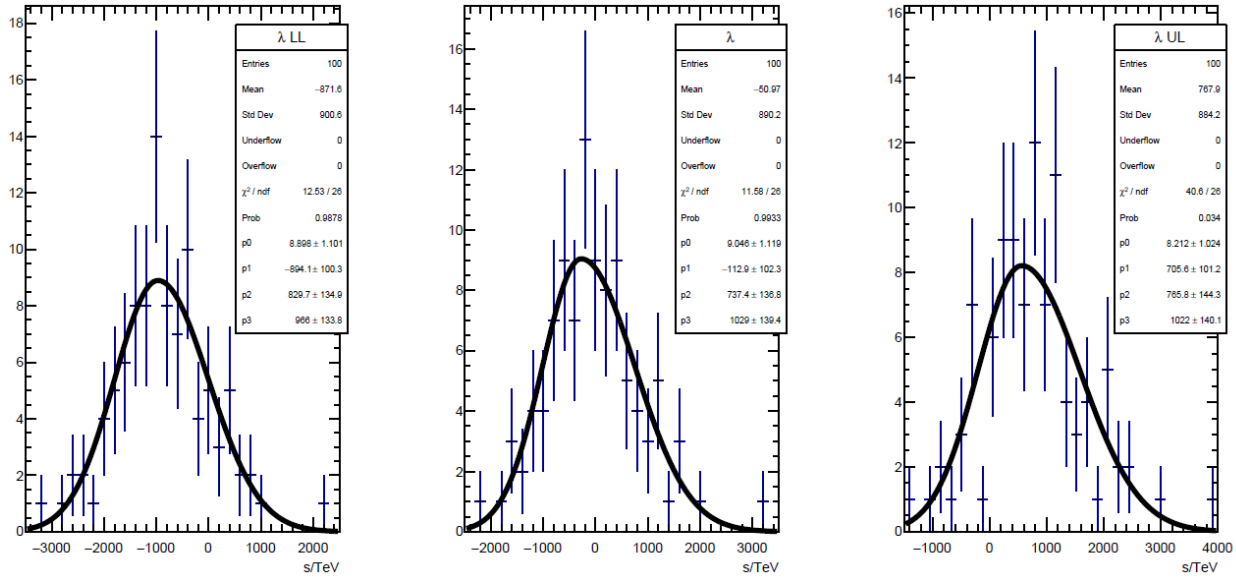

Figure 8: Histogram of the time shift value that maximises the likelihood for each of the 100 simulations, fitted with an asymmetrical Gaussian distribution. *Left*: lower limit of the time shift, *Center*: time shift, *Right*: upper limit of the time shift.

To check whether the simulation can reconstruct the lag properly, we can inject a fake LIV effect. Figures 9 and 10 show the same plots as the two above, but with a fake 2000 s/TeV lag introduced to the simulation. The resulting likelihood value plot shifts to the new minimum around 2000 s/TeV. This is expected since we introduced the same amount of fake shift. The mean is also shifted as expected, along with the upper and lower limits. From this test, we can conclude that the software can recreate the LIV effect.

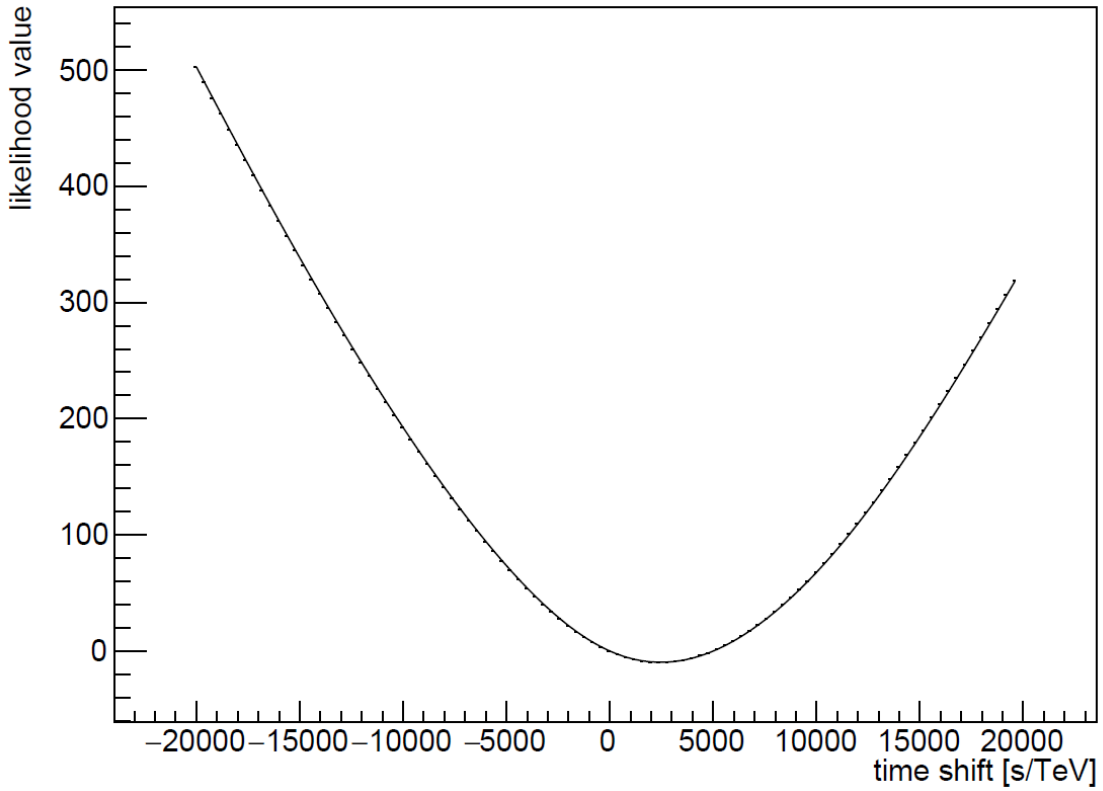

Figure 9: Likelihood value with respect to the timeshift for the example `LIVelihood simulation` of PKS 2155-304 data with the injected time shift of 2000 s/TeV.

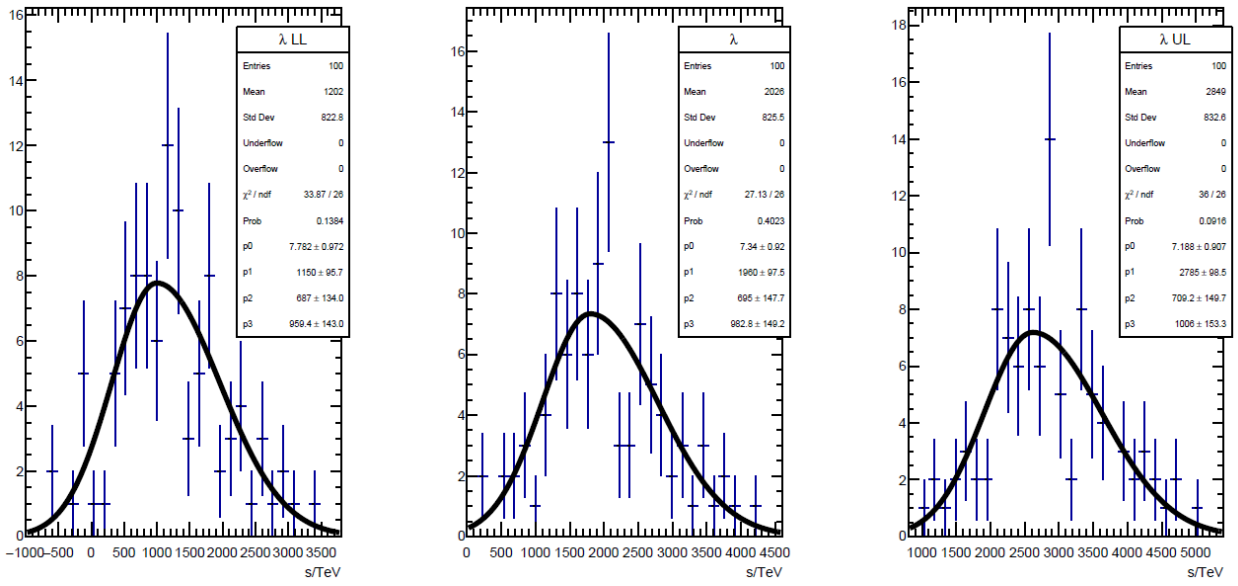

Figure 10: Histogram of the time shift value that maximises the likelihood for each of the 100 simulations with injected time shift of 2000 s/TeV, fitted with an asymmetrical Gaussian distribution. *Left*: lower limit of the time shift, *Center*: time shift, *Right*: upper limit of the time shift

5.2 Markarian 421 analysis

We preformed the analysis on 50 simulations. Optimal analysis is preformed on at least 1000 simulations, but due to hardware limitations we were able to do only 50. The way `LIVelihood` is currently written, it uses more and more RAM as it preforms the simulations. After a while, it uses more than the maximum available RAM and freezes, resulting in a failed simulation run. Because of this the maximum number of simulations that we could do for some functions was 50 and because we want to compare the different functions with each other all the results needed to have the same number of simulations. While this did not result in the most accurate recreation of time shift, we were still able to compare the results between different functions used for creating the light curve template, and that was the goal of this thesis.

With the available hardware, we managed to make up to 100 simulations for the light curve templated created by the four Gaussian distributions. This result is included at the end of this chapter to illustrate the difference more simulation makes on the final result, and to show that the light curve template created by four Gaussian distributions is more efficient in terms of computing power needed than the rest. For the direct comparison of the simulation results, we only used the results from the 50 simulation runs.

5.2.1 Four Gaussian distributions

Figure 11 shows the likelihood value with respect to the time shift for the light curve template created with four Gaussian distributions. The histograms showing the value of the time shift that maximised the likelihood, along with the upper and lower limits, are shown on Figure 12. The mean values for the time shift and its upper and lower limits are given in Table 5. The simulations took about 2 hours to compute. Using Equation (4) we calculated the lower limit for the energy at which the effects of quantum gravity become significant for the linear term:

$$E_{\mathrm{QG}_1}^{(G)} = 2.48557 \cdot 10^{17}\mathrm{GeV} \tag{18}$$

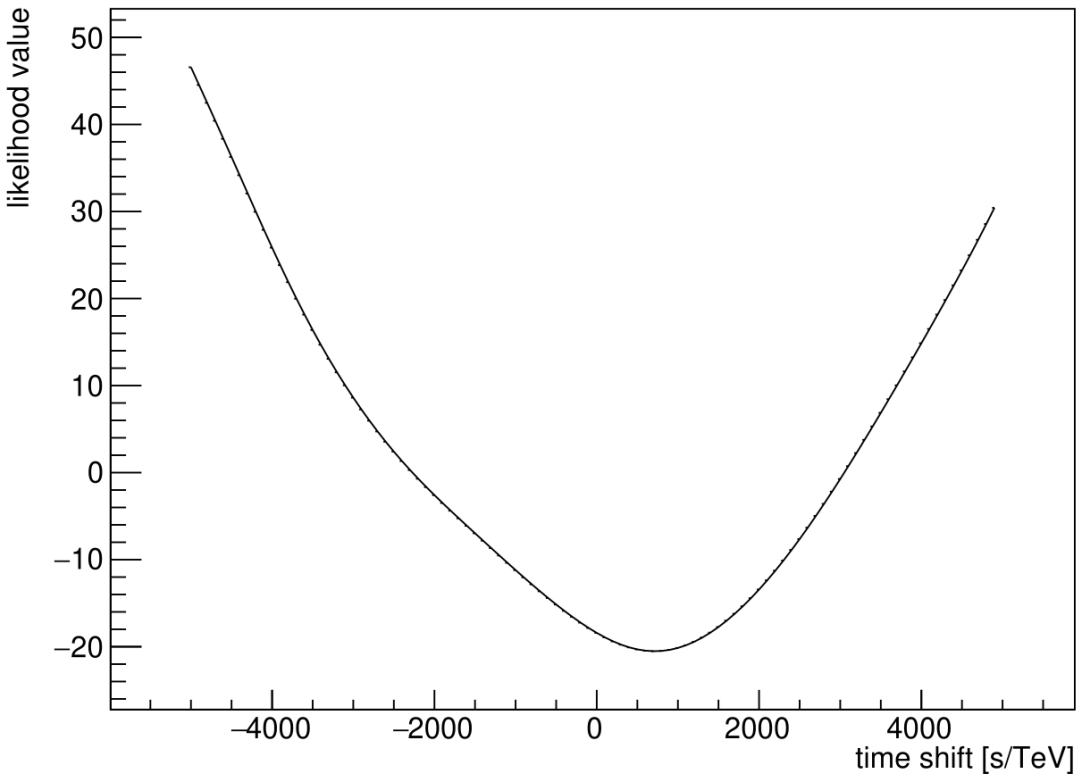

Figure 11: Likelihood value with respect to the timeshift for the light curve template created with four Gaussian distributions.

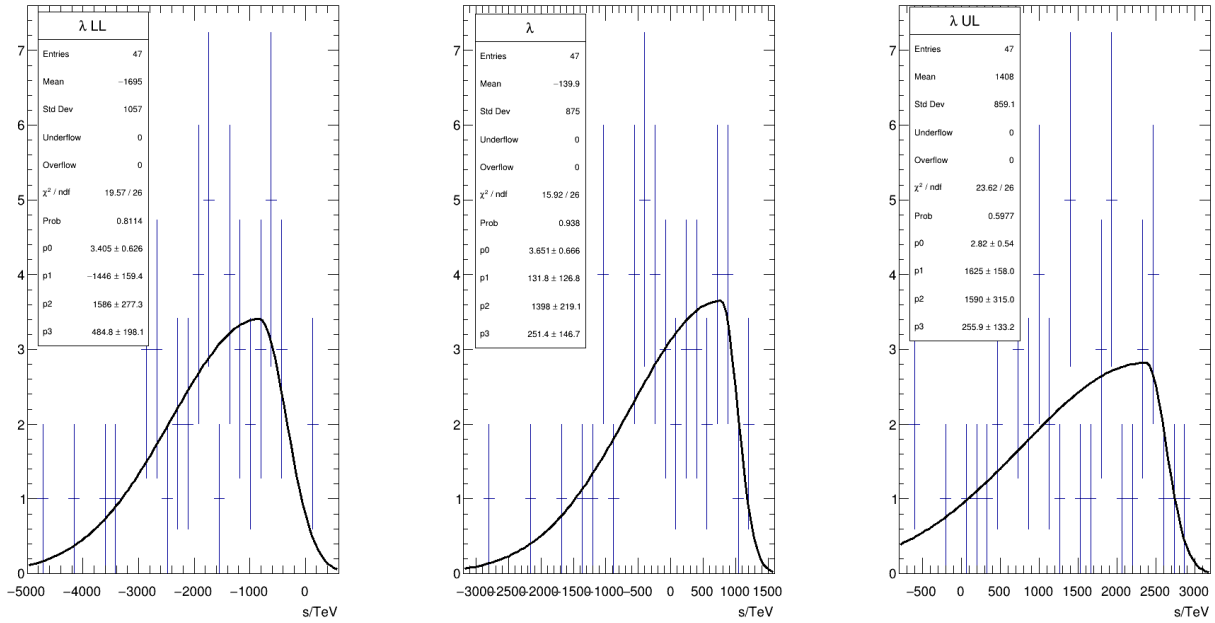

Figure 12: Histogram of the time shift value that maximises the likelihood for the light curve template created with four Gaussian distributions, fitted with an asymmetrical Gaussian distribution. *Left*: lower limit of the time shift, *Center*: time shift, *Right*: upper limit of the time shift.

5.2.2 Three skewed Gaussian distributions

The resulting likelihood value with respect to the time shift for the light curve template created with three skewed Gaussian distributions is shown on Figure 13. The function is very flat around the minimum and does not follow the expected parabolic shape. In the simulations, only a few functions had a converging minimum, which was not enough to create a distribution of the time shift or its limits. The simulation also took a little over 8 hours to compute. From this, we concluded that the most likely cause for the minimization to not converge was the complexity of the function used to create the light curve template. It is possible that with more simulations, more minimums would converge, and a distribution could be created.

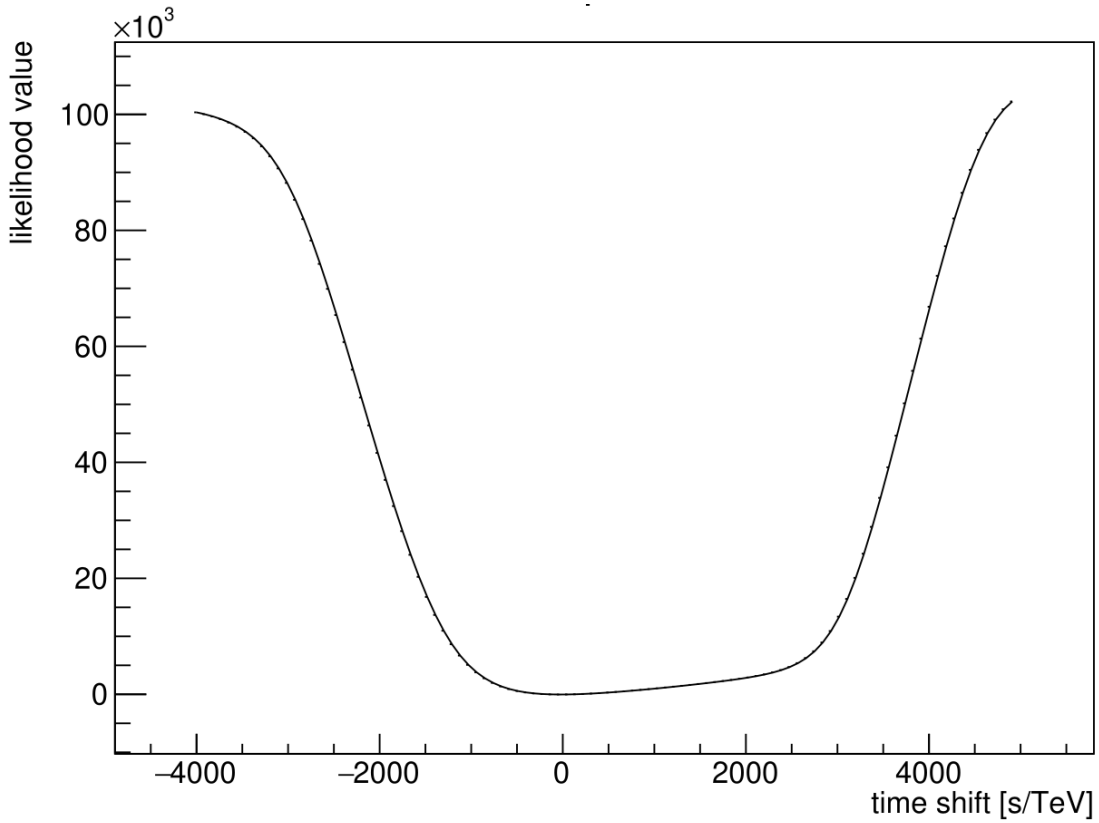

Figure 13: Likelihood value with respect to the timeshift for the light curve template created with three skewed Gaussian distributions.

5.2.3 Four Cauchy distributions

The last simulation used the light curve template created by the four Cauchy distributions. Figure 14 shows the likelihood value with respect to the time shift. The histograms showing the value of the time shift that maximised the likelihood along with the upper and lower limits are shown on Figure 15. The mean of the time shift value with its upper and lower limits is shown in the Table 5. The simulation took about 4.5 hours to compute.

The lower limit of the energy at which the quantum gravity effects become significant for the linear term calculated from λ is:

$$E_{\mathrm{QG}_1}^{(C)} = 3.11314 \cdot 10^{17}\mathrm{GeV} \tag{19}$$

Comparing the results from the four Gaussian distributions and four Cauchy distributions, we concluded that the four Gaussian distributions model had lower uncertainties on the time shift and its limits, and had a faster computing time by about 44.44 %. The 95 % confidence intervals for both models are comparable.

Table 5: Results of the `LIVelihood` simulations using light curves created by: i) four Gaussian distributions, ii) four Cauchy distributions, iii) three skewed Gaussian distributions. $\lambda_{\rm LL}$: lower limit of the time shift, λ: time shift, $\lambda_{\rm UL}$ upper limit of the time shift, $\chi^2_{\rm LL}$: χ^2 result of the asymmetrical Gaussian distribution fit on the histogram of $\lambda_{\rm LL}$, χ^2: χ^2 result of the asymmetrical Gaussian distribution fit on the histogram of λ, $\chi^2_{\rm UL}$: χ^2 result of the asymmetrical Gaussian distribution fit on the histogram of $\lambda_{\rm UL}$, $\rm p-value_{LL}$: p-value result of the asymmetrical Gaussian distribution fit on the histogram of $\lambda_{\rm LL}$, p-value: p-value result of the asymmetrical Gaussian distribution fit on the histogram of λ, $\rm p-value_{UL}$ result of the asymmetrical Gaussian distribution fit on the histogram of $\lambda_{\rm UL}$, N_{par}: number of parameter of the function used to create the light curve template.

Parameter	four Gaussian distributions	four Cauchy distributions	three skewed Gaussian distributions
$\lambda_{\rm LL}$	-1695 ± 1057	-1523 ± 1307	-
λ	-139.9 ± 875	-76.22 ± 971	-
$\lambda_{\rm UL}$	1408 ± 859.1	1416 ± 1276	-
$\chi^2_{\rm LL}$	19.57	30.33	-
χ^2	15.92	16.81	-
$\chi^2_{\rm UL}$	23.62	26.42	-
$\rm p-value_{LL}$	0.8114	0.2543	-
p-value	0.938	0.9147	-
$\rm p-value_{UL}$	0.5977	0.44	-
N_{par}	12	12	12

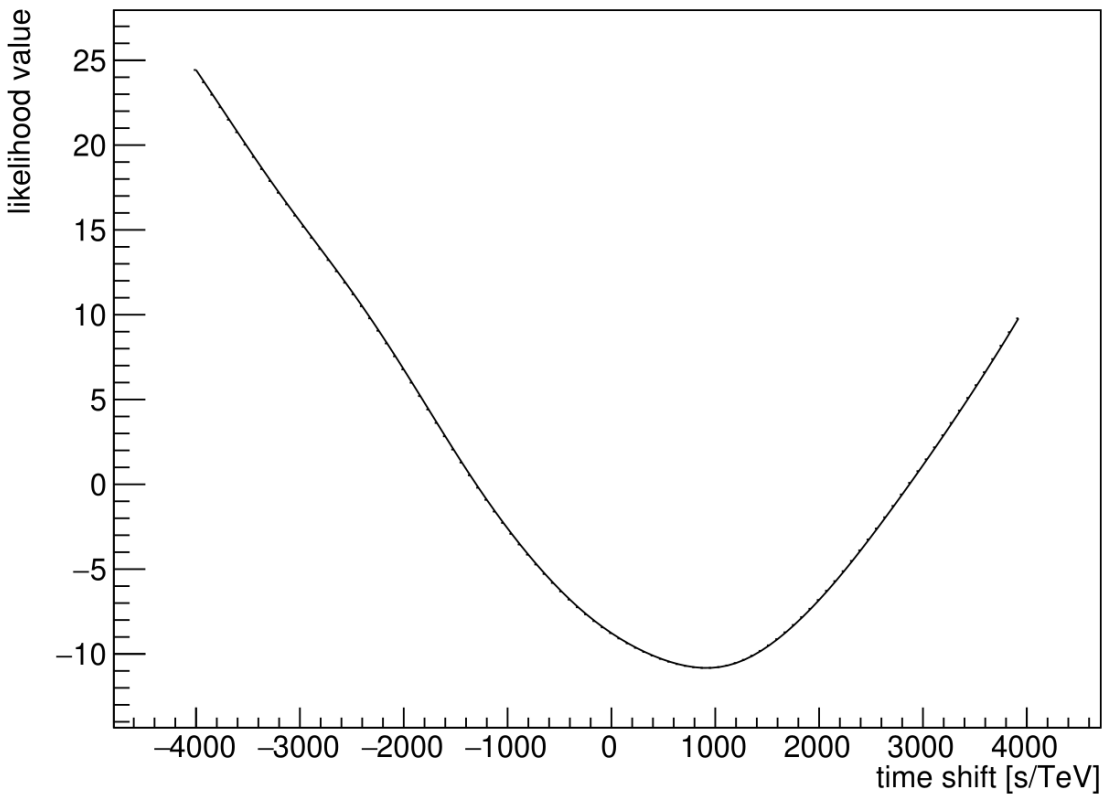

Figure 14: Likelihood value with respect to the timeshift for the light curve template created with four Cauchy distributions.

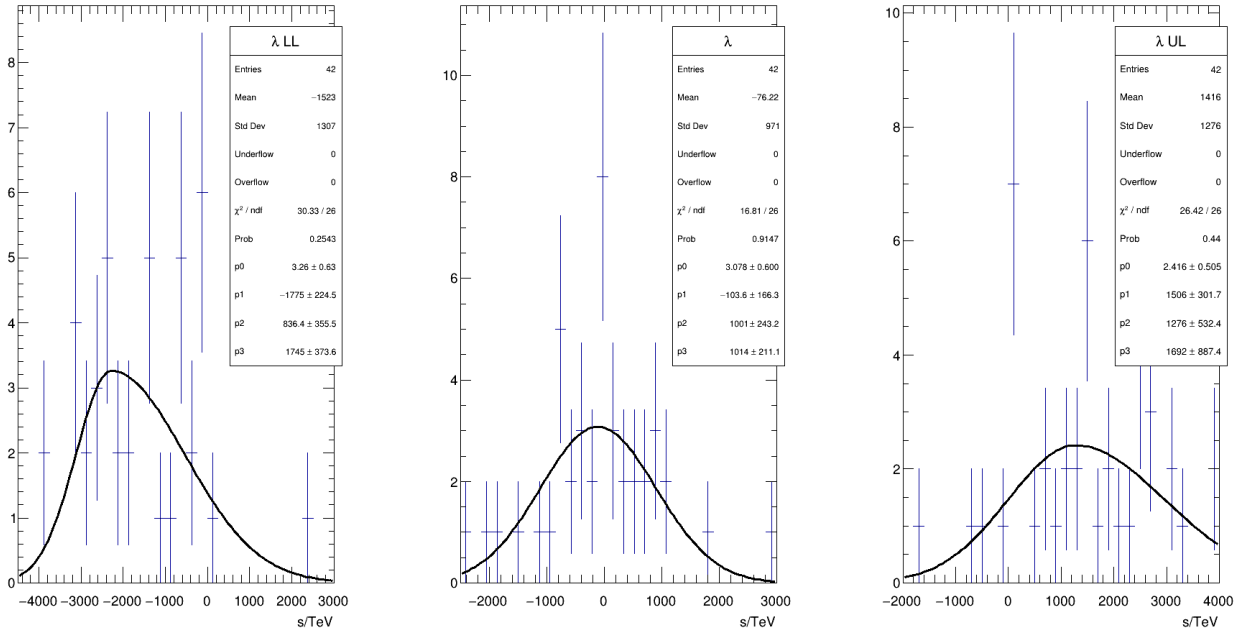

Figure 15: Histogram of the time shift value that maximises the likelihood for the light curve template created with four Cauchy distributions, fitted with an asymmetrical Gaussian distribution. *Left*: lower limit of the time shift, *Center*: time shift, *Right*: upper limit of the time shift.

5.2.4 Additional results

As mentioned before, for the light curve template created using the four Gaussian distributions, we managed to complete 100 simulations. The likelihood value with respect to the time shift is shown on Figure 16 and the histograms showing the value of the time shift that maximised the likelihood along with the upper and lower limits are shown on Figure 17. The resulting mean of the time shift and its upper and lower limits are:

$$\begin{aligned} \lambda_{\mathrm{LL}} &= -1542 \pm 997.1 \\ \lambda &= 42.58 \pm 804.1 \\ \lambda_{\mathrm{UL}} &= 11590 \pm 938.9 \end{aligned} \tag{20}$$

The lower limit of the energy at which the quantum gravity effects become significant for the linear term calculated from λ is:

$$E_{\mathrm{QG}_1} = 2.6614 \cdot 10^{17}\mathrm{GeV} \tag{21}$$

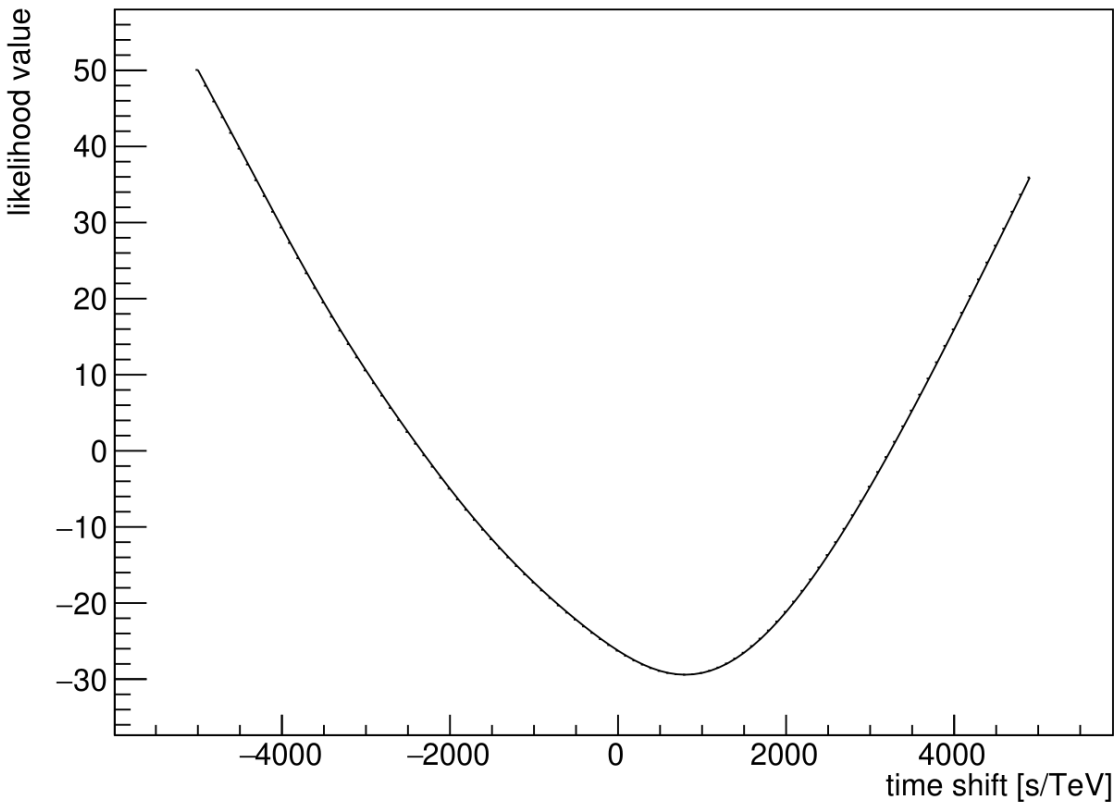

Figure 16: Likelihood value from 100 simulations with respect to the timeshift for the light curve template created with four Gaussian distributions.

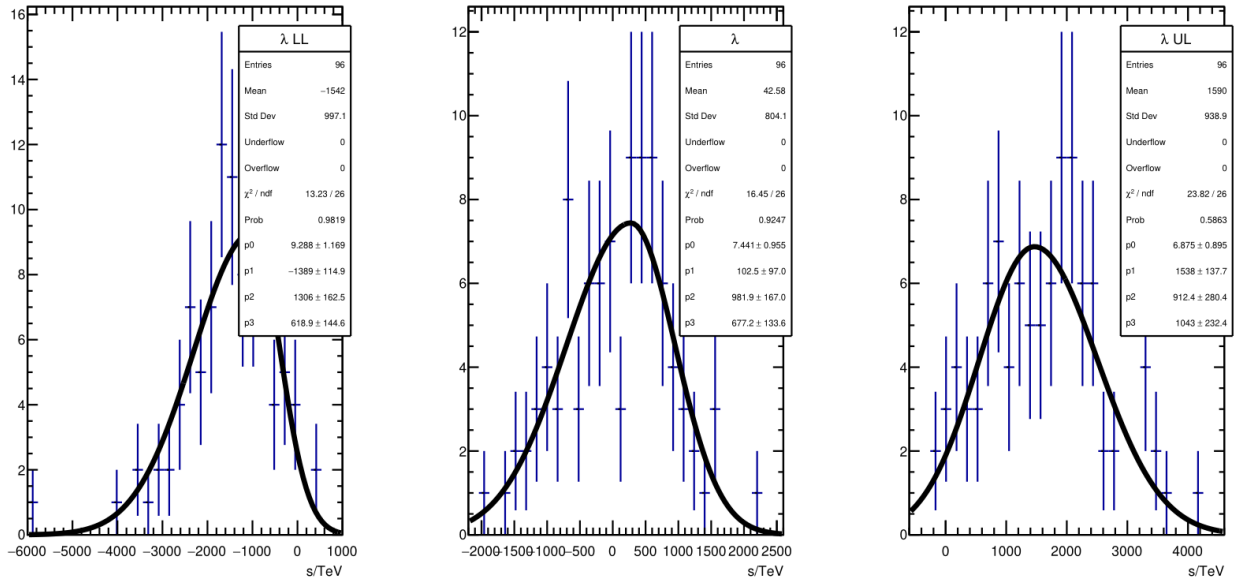

Figure 17: Histogram of the time shift value that maximises the likelihood from 100 simulations for the light curve template created with four Gaussian distributions, fitted with an asymmetrical Gaussian distribution. *Left*: lower limit of the time shift, *Center*: time shift, *Right*: upper limit of the time shift.

6 CONCLUSION

Measurements of quantum gravity are challenging because of the energy scale at which the effects of quantum gravity are expected to manifest. In spite of this, by utilising some of the proposed quantum effects, such as fluctuations of space-time on the Planck scale, we could make measurements of quantum gravity at much lower energy scales. By modelling the effects of space-time fluctuations as a modification of the photon dispersion relation, we could observe the LIV effect at energies much lower than the Planck scale.

In this thesis, we focused on checking how the choice of the function used to reconstruct the light curve template affects the maximum likelihood analysis done by `LIVelihood` simulations. Using the gamma rays from Markarian 421 observed by MAGIC telescopes on the night of 24 to 25 of April 2014 we recreated the light curve template by fitting five different functions. Further analysis with the recreated light curve templates was done on simulations of the observed data. Before making the fit, we binned the data into ON and OFF regions. By subtracting the ON and OFF regions, we got an approximated number of gamma rays coming from the signal. The fit was then done on the gamma rays in the 100 to 200 GeV energy range. This gave us a good number of gamma rays to fit while also keeping the LIV effect negligible.

For the KDE, we were not able to find a good justification for the choice of the bandwidth parameter. Making the bandwidth too high would hide a lot of the structure in the data, and making it too small makes the resulting fit show more variation than present in the data. Because of this KDE was not used in the final `LIVelihood` simulations. The fit using Fourier series also did not manage to give satisfying results for the use in `LIVelihood` simulations. The fit was not able to recreate the structure of the light curve and had big deviation on certain points. The other three fits: sum of Gaussian distributions, sum of skewed Gaussian distributions and sum of Cauchy distributions managed to capture the light curve variations with more accuracy. As seen in table 4 all the fits had a similar χ^2 value, so we could compare the simulation results from their respective light curves.

In the end, for the light curve created with three skewed Gaussian distributions not enough of the minimums were convergent, so the distribution could not have been calculated. The most likely cause is the complexity of the function used to create the light curve template. That left us with the four Gaussian distributions and the four Cauchy distributions models for comparison. While the simulations using both models managed to calculate

the time shift value with its upper and lower limits, the simulation with the four Gaussian distributions computed much faster. In addition, the four Gaussian distributions model had lower uncertainties on the time shift and its limits, in comparison to the four Cauchy distributions model. The 95 % confidence intervals of both models were compareble. Finally, for the four Gaussian distributions model we managed to compute up to 100 simulations, making it the most efficient model in terms of computing power needed. The lower limits for the energy at which the effects of quantum gravity become significant in the linear term were calculated as $E^{(G)}_{\mathrm{QG}_1} = 2.48557 \cdot 10^{17}\,\mathrm{GeV}$ for the four Gaussian distributions model and $E^{(C)}_{\mathrm{QG}_1} = 3.11314 \cdot 10^{17}\,\mathrm{GeV}$ for the four Cauchy distributions model.

For future analysis, these simulations can be repeated but with at least 1000 simulations for each function. That would give a more accurate time shift calculation and might give some results even for the three skewed Gaussian distributions model. In addition, with the right justification for the bandwidth parameter of the KDE, the simulations could be done with the light curve template created with KDE.

Bibliography

[1] Carlo Rovelli and Lee Smolin. Loop space representation of quantum general relativity. *Nuclear Physics B*, 331(1):80–152, 1990. ISSN 0550-3213.

[2] Carlo Rovelli. Quantum gravity. In Jeremy Butterfield and John Earman, editors, *Philosophy of Physics*, Handbook of the Philosophy of Science, pages 1287–1329. North-Holland, Amsterdam, 2007.

[3] Daniele Oriti. Spacetime geometry from algebra: spin foam models for non-perturbative quantum gravity. *Reports on Progress in Physics*, 64(12):1703–1757, nov 2001. doi: 10.1088/0034-4885/64/12/203.

[4] M. Niedermaier and M. Reuter. The asymptotic safety scenario in quantum gravity. *Living Reviews in Relativity*, 9(5), dec 2006. doi: 10.12942/lrr-2006-5.

[5] J. Ambjørn, A. Görlich, J. Jurkiewicz, and R. Loll. Nonperturbative quantum gravity. *Physics Reports*, 519(4-5):127–210, oct 2012. doi: 10.1016/j.physrep.2012.03.007.

[6] Gary T Horowitz. Spacetime in string theory. *New Journal of Physics*, 7:201–201, sep 2005. doi: 10.1088/1367-2630/7/1/201.

[7] D. J. Bird, S. C. Corbato, H. Y. Dai, J. W. Elbert, et al. Detection of a cosmic ray with measured energy well beyond the expected spectral cutoff due to cosmic microwave radiation. *The Astrophysical Journal*, 441:144, mar 1995. doi: 10.1086/175344.

[8] F. Halzen, R.A. Vázquez, T. Stanev, and H.P. Vankov. The highest energy cosmic ray. *Astroparticle Physics*, 3(2):151–156, 1995. ISSN 0927-6505. doi: https://doi.org/10.1016/0927-6505(94)00038-5.

[9] Zhen Cao, F. A. Aharonian, Q. An, et al. Ultrahigh-energy photons up to 1.4 peta-electronvolts from 12 γ-ray galactic sources. *Nature*, 594(7861):33–36, Jun 2021. ISSN 1476-4687. doi: 10.1038/s41586-021-03498-z.

[10] J. Bolmont, S. Caroff, M. Gaug, et al. First combined study on lorentz invariance violation from observations of energy-dependent time delays from multiple-type gamma-ray sources. i. motivation, method description, and validation through simulations of

h.e.s.s., MAGIC, and VERITAS data sets. *The Astrophysical Journal*, 930(1):75, may 2022. doi: 10.3847/1538-4357/ac5048.

[11] J. Albert, E. Aliu, H. Anderhub, L.A. Antonelli, P. Antoranz, M. Backes, C. Baixeras, et al. Probing quantum gravity using photons from a flare of the active galactic nucleus markarian 501 observed by the MAGIC telescope. *Physics Letters B*, 668(4):253–257, oct 2008. doi: 10.1016/j.physletb.2008.08.053.

[12] N. Aghanim, Y. Akrami, M. Ashdown, J. Aumont, et al. Planck 2018 results. VI. Cosmological parameters. *Astronomy & Astrophysics*, 641:A6, sep 2020. doi: 10.1051/0004-6361/201833910.

[13] Uri Jacob and Tsvi Piran. Lorentz-violation-induced arrival delays of cosmological particles. *Journal of Cosmology and Astroparticle Physics*, 2008(01):031, jan 2008. doi: 10.1088/1475-7516/2008/01/031.

[14] Tomislav Terzić, Daniel Kerszberg, and Jelena Strišković. Probing quantum gravity with imaging atmospheric cherenkov telescopes. *Universe*, 7(9):345, sep 2021. doi: 10.3390/universe7090345.

[15] James Frederick. *Statistical Methods in Experimental Physics*. "World Scientific Publishing Co. Pte. Ltd", 2008.

[16] F. Krennrich, H. M. Badran, I. H. Bond, S. M. Bradbury, et al. Cutoff in the TeV energy spectrum of markarian 421 during strong flares in 2001. *The Astrophysical Journal*, 560 (1):L45–L48, oct 2001. doi: 10.1086/324221.

[17] V.P. Fomin, A.A. Stepanian, R.C. Lamb, D.A. Lewis, M. Punch, and T.C. Weekes. New methods of atmospheric cherenkov imaging for gamma-ray astronomy. i. the false source method. *Astroparticle Physics*, 2(2):137–150, 1994.

[18] L. Nogués. *Constraints on Lorentz Invariance Violation through the study of energy-dependent photonic time dispersion utilizing observations from current gamma-ray instruments*. Phd thesis, University of Zaragoza, Department of theoretical physics, 2018.

[19] Sami Caroff, Anna Campoy-Ordaz, Ugo Pensec, Cyann Plard, and Alessandro Armando Vigliano. Search for Lorentz Invariance Violation with time-lag on gamma-

ray Cherenkov Telescope data: From the data to the time lag constraints. *PoS*, QG-MMSchools:009, 2023. doi: 10.22323/1.440.0009.